

CFD analysis of the flow-field scale-up influence on the electrodes performance in a PEFC[☆]

G. Squadrito^{*}, O. Barbera, I. Gatto, G. Giacoppo, F. Urbani, E. Passalacqua

CNR-ITAE, via Salita S. Lucia sopra Contessen. 5, 98126 S. Lucia, Messina, Italy

Received 30 November 2004; accepted 28 December 2004

Available online 8 March 2005

Abstract

A computational fluid dynamic (CFD) analysis was used as a useful tool to obtain numerical relationships among similar flow-field designs having different active areas. Assuming that, at fixed current density, the porous layer velocity distribution calculated for the smallest size geometry was the optimal, a scale-up methodology has been proposed and implemented in software. It allows acquisition of the scaled-up flow-field by multiplying the reference cell parameters by suitable factors (scale factors). A calibration methodology has also been proposed by the introduction of a feedback factor evaluated by CFD analysis. A first application of this procedure has been carried out to scale-up a 5–125 cm² cell.

© 2005 Elsevier B.V. All rights reserved.

Keywords: CFD; Scale-up; Fuel cell; Flow-field design

1. Introduction

The polymer electrolyte fuel cell (PEFC) is becoming an interesting power source in various application fields, from portable units to large stationary systems. This wide range in power output implies a great variation of the active area size depending on the application. Generally, the scale-up of flow-field geometry from the lab scale single cell to the stack gives performance losses due to the fluid dynamic changes introduced by the scaling procedure. In the PEFC, both hydrogen and alcohol fed, the interaction between the flow-field and the electrode diffusion layer plays a primary role [1–3]. Then when a cell configuration (flow-field plus electrode) has been optimised in the laboratory, the maintaining of the reactant distribution and consequently of the performance requires a new optimisation, increasing of the realisation time and the cost of the system.

Availing ourselves of computational fluid DYNAMIC (CFD) analysis, a computer aided fuel-cell design methodology was realised able to reduce the performance loss and to limit the number of lab-tests. The method involves the parameterisation and the automatic generation algorithm of the most common flow-fields as previously reported [4].

In the present work, the algorithm was used as part of a computer aided selection method and flow-field scale-up. The design selection methodology is explained by describing the main program, the subroutines and their interaction separately. The software application to the scale-up from a starting cell of 5–125 cm² is also reported. It was observed that the input variable constrains influence the results. A method for algorithm calibration was introduced by means of a check parameter taking into account the mass transfer towards the electrode. The CFD analysis has been used to evaluate this parameter and the methodology general aspects.

2. Design selection method

An automatic scaling-up design procedure demands the definition of parameters describing the object and their vari-

[☆] This paper was presented at the 2004 Fuel Cell Seminar, San Antonio, TX, USA.

^{*} Corresponding author. Tel.: +39 090624231; fax: +39 090624247.

E-mail address: gaetano.squadrito@itae.cnr.it (G. Squadrito).

Nomenclature

MEA geometrical parameters

AMEA electrode surface area
LMEA MEA width

Flow-path parameters

LCAN sub-channel width
LCOS rib width
HCAN channel height
NDIV sub-channel number

Flow-path generation parameters

Coll “connection module” height
Hmea MEA height
Lmea MEA width updated value
Lser serpentine equivalent width
Lung “base module” height
N reference value for modules repetitions

ation range (constrains). In the case of fuel cells, the following parameters related to the channel gas flow path have been defined: meander type (serpentine, ribbed, etc.), active area surface and geometry (square, rectangular, etc.), section (square, circular, triangular, etc.) width and depth of the channels, rib width, etc. In addition to geometrical characteristics, fluid dynamic properties have to be also considered, because a correct reactant distribution over the electrode active area is fundamental to reach a good fuel cell performance [1–3]. Starting from the above mentioned parameters the computer aided scale up method permits us to obtain in the active area a fixed range of the flow-field giving performance as close as possible to the reference.

The developed software consists of four routines (Fig. 1), the main, the flow-field generation software (FGS), the selection algorithm software (SAS) and the post-graphic output (PGO).

The MAIN routine elaborates the active area within the selected range and operative conditions inputs and sends the calculated construction parameters to the FGS that, according to the methodology explained in [4], generates all the possible serpentine like flow-fields: single (SS), ribbed (RS) and multi-serpentine (MS). Then, the SAS subroutine selects the design which matches geometrical and fluid dynamics constraints. At each i th step the selected flow-field is stored in a database and successively used for diagram generation by the post-processing graphical output (PGO) routine. PGO also generates the scale factor and diagrams as a function of the cell active area.

A conventional single serpentine flow-pattern was selected as the sample case because it is the most common flow-field in the PEFC. In particular, the commercially available 5 cm^2 active area used for the lab test cell was a single serpentine with a rectangular channel of 1 mm in width and 1 mm in depth and 10 180° turns (11 passages total). As a sample case

the cathode side of an H_2/air cell was considered, and the selected operative conditions were: $J = 500 \text{ mA cm}^{-2}$ (current density), $T = 80^\circ \text{C}$ (operating temperature), $p = \text{room pressure}$, $\text{RH} = 100\%$ (air relative humidity), $x = 1.5/2$ (H_2/air stoichiometric ratio). According to equation and symbols used in reference [4] (see Appendix A), the assumed operative conditions are used to calculate the stream inlet velocity as follows:

$$v_{\text{med}_r} = \frac{1}{\rho A_{\text{in}}} M_r \frac{J \text{ AMEA}}{nF} \quad (2.1)$$

where ρ is the stream inlet density, A_{in} is the flow-field inlet area, M_r represents the reactant molecular weight, F is the Faraday's constant, n the electrons number involved in the semi-reaction and AMEA is the total active area.

In Fig. 2 the reference flow-field is shown and its characteristics reported in the table on the right side, where the v_{med} and other fluid dynamic parameters values are calculated at the selected operative conditions.

2.1. MAIN routine

The MAIN routine spans the active area from AMEA_{min} to AMEA_{max} with a defined increment, ΔAMEA . MAIN input variables are the cell operative conditions, the total MEA active area range and the step to be used (Table 1). For each AMEA_i the routine calculates all the variables to be send to the FGS routine.

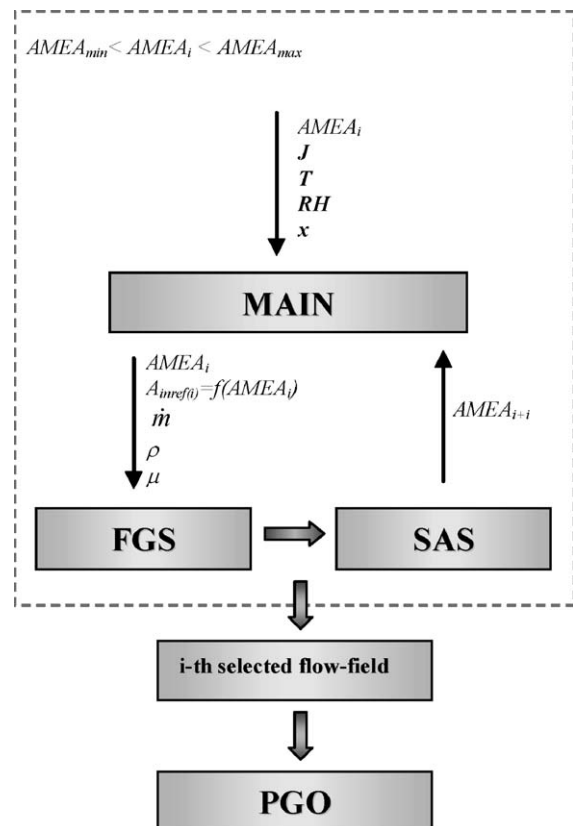
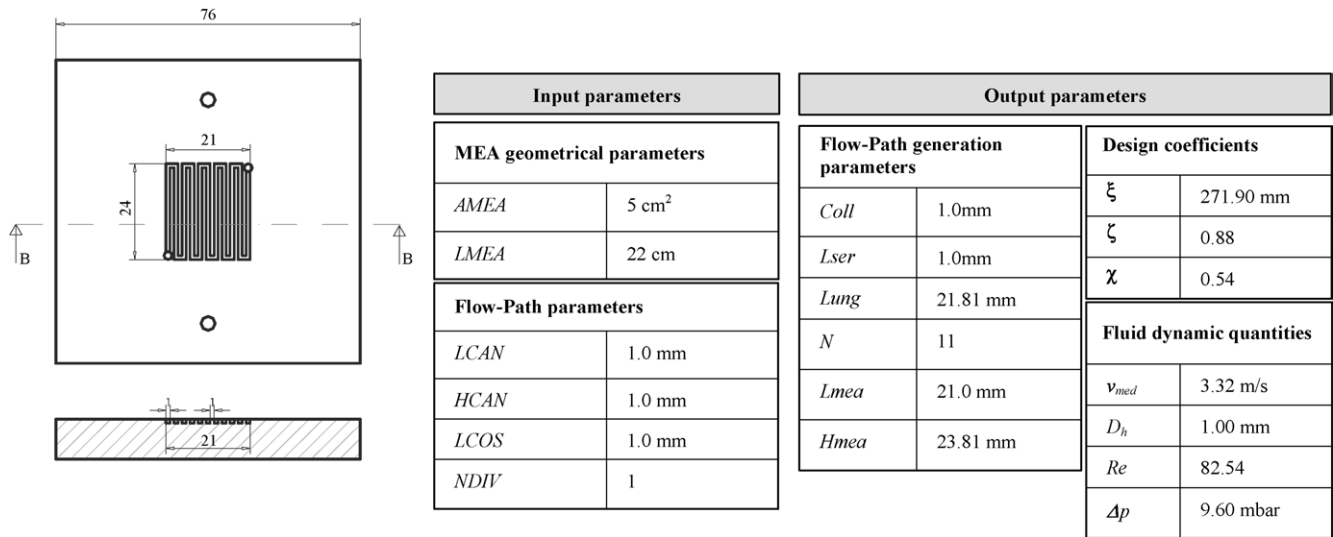


Fig. 1. Scale-up software flowchart.

Fig. 2. Sketch of 5 cm² reference cell and tables of its parameter values.

The inputs are used to calculate the reactant stream mass flow rate and its thermodynamic properties, namely fluid density and fluid viscosity and *i*th reference inlet area:

$$A_{in,ref(i)} = \frac{\dot{m}_i}{\rho v_{med,ref}} \quad (2.2)$$

where $v_{med,ref}$ represents the average inlet velocity of the reference cell, therefore $A_{in,ref(i)}$ stands for the channels cross-sectional area that gives an inlet velocity value equal to that of the reference cell.

The number of iterations depends on $AMEA_{min}$, $AMEA_{max}$ and $\Delta AMEA$ as follows:

$$n_{cycles} = \left(\frac{AMEA_{max} - AMEA_{min}}{\Delta AMEA} \right) + 1 \quad (2.3)$$

Fluid density and viscosity were calculated by simple mathematic media assuming that the stream is a mixture of two perfect gas, air and water vapour.

2.2. Flow-field generation software FGS

The methodology for automatic serpentine like flow-field generation previously evolved [4], was implemented to allow

Table 1
Main program input and output variables

Input	Output
Total active area max value, $AMEA_{max}$	<i>i</i> th total active area, $AMEA_i$
Total active area min value, $AMEA_{min}$	Ref. inlet area, $A_{in,ref(i)}$
Total active area step value, $\Delta AMEA$	
Operative conditions	
Current density, J	Gas flow rate, \dot{m}_i
Operating temperature, T	Fluid density, ρ
Back-pressure, p	Fluid viscosity, μ
Relative humidity, RH	
Stoichiometric ratio, x	

the generation of all the possible designs having geometric characteristics inside the defined ranges. The FGS takes into account the outputs coming from the MAIN (see Table 2) and the geometric constrains to calculate the solution matrix dimensions by the following equations:

$$n_r = \text{int} \left(\frac{A_{in,max}}{\Delta A_{in,i}} \right) \quad (2.4a)$$

$$n_c = \frac{NDIV_{max}}{\Delta NDIV} \quad (2.4b)$$

Table 2
FGS parameters

Input	Output
Active area parameters	Flow-path parameters
Electrode surface area, $AMEA_i$	Sub-channel width, $LCAN_i$
Ref. <i>i</i> th inlet area, $A_{in,ref(i)}$	Sub-channel number, $NDIV_i$
Inlet steam characteristics	Flow-path generation parameters (FGPs)
Gas flow rate, \dot{m}	MEA width, $Lmea_i$
Fluid density, ρ	MEA height, $Hmea_i$
Fluid viscosity, μ	Reference value for modules repetitions, N_i
Flow-path parameters	“Connection module” height, $Coll_i$
Channel height (fixed), $HCAN$	Serpentine equivalent width, $Lser_i$
Rib width (fixed), $LCOS$	“Base module” height, $Lung_i$
	Design coefficients (DCs)
	“Unrolled” serpentine length, ξ_I
	MEA aspect ratio, ζ_I
	Covering factor, χ_I
	Fluid dynamic quantities (FDQ)
	Average channel velocity, v_{med}
	Hydraulic diameter, D_h
	Reynolds number, Re_i
	Total serpentine pressure drop, Δp_i

where $A_{in_{max}}$ and $NDIV_{max}$ are evaluated as follows:

$$A_{in_{max}} = kA_{in_{ref(i)}} \quad \text{with } 0 < k \leq 1 \quad (2.5)$$

$$NDIV_{max} = \text{int}(A_{in_{max}}) + \delta \quad (2.6)$$

where

$$\delta = \begin{cases} 0 & \text{if } \text{dec}(A_{in_{max}}) \leq 0.5 \\ 1 & \text{if } \text{dec}(A_{in_{max}}) \geq 0.5 \end{cases}$$

Eqs. (2.4a) and (2.4b) represent the rows and columns number of the solution matrix, respectively, whereas Eq. (2.5) gives the maximum value of cross-sectional inlet area as a multiple of $A_{in_{ref(i)}}$, and Eq. (2.6) the number of channel subdivisions ($NDIV_{max}$).

Consequently the number of possible designs is:

$$n_{sol} = n_r n_c \quad (2.7)$$

To reduce the solution matrix dimension the channel height (HCAN) and rib width (LCOS) were considered as fixed values, while the sub-channels number ($NDIV_i$) and width ($LCAN_i$) vary to cover the i th inlet area:

$$NDIV_i = NDIV_{min} + j\Delta NDIV, \quad j = 1-n_c,$$

$$A_{in_i} = A_{in_{min}} + l\Delta A_{in_i}, \quad l = 1-n_r \quad (2.8)$$

where $NDIV_{min}$ is the minimum allowed value fixed (=1 for simple serpentine), $\Delta NDIV$ represents the increment (in our case = 1), $A_{in_{min}}$ is a percentage of $A_{in_{ref(i)}}$ and ΔA_{in_i} represents the channel cross-section inlet area increment.

Given A_{in_i} and $NDIV_i$, $LCAN_i$ and the other output parameters are immediately determined for each iterative cycle as:

$$LCAN_i = \frac{A_{in_i}}{NDIV_i HCAN} \quad (2.9)$$

Thus the software for each A_{in_i} that is $A_{in_{min}} \leq A_{in_i} \leq A_{in_{max}}$ calculates the flow path generation parameters (FGPs) and the design coefficient (DCs) by varying $NDIV_i$.

The inputs and outputs of FGS are listed in Table 2. FGPs, DCs and FDQ were calculated by using equations described in [4] and listed in Appendix A.

2.3. Selection software (SAS)

Even if the solutions coming from the FGS are mathematically correct not everything can be practically realised, so that the SAS provides a solution filtering on the basis of geometrical constraints.

The first constraint considers the maximum usable sub-channel width, in fact the MEA flexibility causes a penetration of the electrode into the channels obstructing the gas flow path. So that, if the mechanical properties of the MEA are known [5], the suitable sub-channel width could be fixed, moreover a minimum value for the sub-channel must also

be set to avoid important pressure losses in the flow-field. Therefore, i th sub-channel width is admitted only if:

$$LCAN_{min} \leq LCAN_i \leq LCAN_{max} \quad (2.11)$$

A sub-channel width proportional to 0.1 mm was fixed for manufacturing reasons, so that the SAS algorithm eliminates all the solutions which do not respect the subsequent condition:

$$LCAN_i \propto 0.1 \quad (2.12)$$

As is well known, the electrode contact area must be maximised to minimise the contact ohmic losses, otherwise a free area needs to assure reactants of diffusion through the electrode backing toward the active catalyst sites. This parameter is taken into account by the covering factor χ which is defined as the free area to total active area ratio, thus for i th solution χ_i value is limited by:

$$\chi_{min} \leq \chi_i \leq \chi_{max} \quad (2.13)$$

Studies of flow-field and electrode diffusion layer interactions [1,2] suggest that the channels gas shorting depends on the total flow-field pressure drop which is related to the serpentine turns number, N . In fact, the N parameter influences the pressure driven mass flow rate through the porous layer, therefore, the SAS imposes that the N parameter for i th generated flow-field is in the range:

$$N_{min} \leq N_i \leq N_{max} \quad (2.14)$$

where N_{min} and N_{max} values are empirically fixed.

A further constraint is imposed from the MEA aspect ratio, ζ , ranging between a ζ_{min} and a ζ_{max} to have the desired active area shape. For the sample case the aspect ratio of the reference cell was chosen.

The SGS provides also a selection of the flow-field type and, for the reported sample case the following selection equations were used:

$$NDIV = 1 \quad (\text{simple serpentine}) \quad (2.15)$$

$$NDIV > 1 \quad \text{and} \quad Coll > Coll_{max} \quad (\text{multiple serpentine}) \quad (2.16)$$

$$NDIV > 1 \quad \text{and} \quad Coll \leq Coll_{max} \quad (\text{ribbed serpentine}) \quad (2.17)$$

in fact the $NDIV$ parameter value is a switch between SS and MS/RS, while the $Coll$ parameter value allows to choose between MS and RS flow-field, the $Coll_{max}$ can be fixed by the user, considering the mechanical MEA properties and flow-path fluid-dynamic aspects.

At this point the fluid dynamic conditions can be imposed to select a unique flow-field design. In the sample case a pressure drop as close as possible to the reference flow-field

pressure drop was required. A pressure drop difference percentage ($\Delta p_i^{\%}$) term representing the variation in pressure drop from the reference value was introduced:

$$\Delta p_i^{\%} = \text{abs} \left(\frac{\Delta p_i - \Delta p_{\text{ref}}}{\Delta p_i} \right) \times 100 \quad (2.18)$$

where the i th component of the $\Delta p^{\%}$ array is estimated by Eq. (2.18).

The final solution is the closest to the reference:

$$\Delta p_{\text{SOL}}^{\%} = \min(\Delta p^{\%}) \quad (2.19)$$

2.4. The PGO software

The PGO software is used to post-process the obtained solution matrix, each solution was characterized by seven dimensionless scale factors.

Among the FGS parameters listed in Table 1 those considered most significant were chosen and the ratio with the corresponding reference value was defined:

$$\alpha_1 = \frac{\text{LCAN}_i}{\text{LCAN}_{\text{ref}}} \quad (2.20)$$

$$\alpha_2 = \frac{\text{NDIV}_i}{\text{NDIV}_{\text{ref}}} \quad (2.21)$$

$$\beta_1 = \frac{\zeta_i}{\zeta_{\text{ref}}} \quad (2.22)$$

$$\beta_2 = \frac{\chi_i}{\chi_{\text{ref}}} \quad (2.23)$$

$$\gamma_1 = \frac{\Delta p_i}{\Delta p_{\text{ref}}} \quad (2.24)$$

$$\gamma_2 = \frac{v_{\text{med}_i}}{v_{\text{med}_{\text{ref}}}} \quad (2.25)$$

$$\gamma_3 = \frac{Re_i}{Re_{\text{ref}}} \quad (2.26)$$

The α_i , β_i , γ_i , factors are related to the serpentine geometry (in Eqs. (2.20) and (2.21)), to the MEA DCs (in Eqs. (2.22) and (2.23)) and to the FDQ (in Eqs. (2.24)–(2.26)) respectively. The scale factors value is the unit when i th solution and its reference correspondent parameters are equal, whereas the minimum and maximum values are strongly dependent on the assigned constrains.

The graphic output of PGO gives an immediate outlook of scale factor variation in respect of active surface area. After constrain calibration, the scale factor graphics furnish all the flow-field scale-up parameters in the suited active area range.

2.5. Algorithm application

It is noticed that the proposed methodology needs to be calibrated because of the output parameters (the scale factors), coming from the PGO, are strongly related to the assigned constrain values. Thus, to select a suitable geometrical and

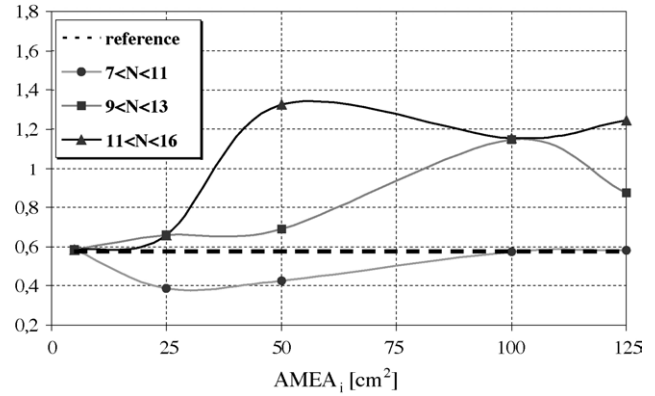


Fig. 3. ψ behaviour vs. cell active area for different N range values.

fluid dynamic constrains range, a feedback parameter has to be introduced. In this work, to apply the algorithm to a sample case, a parameter ψ was introduced and evaluated by CFD analysis according to reference [2]:

$$\psi = \frac{\dot{m}_{\text{el}}}{\dot{m}_{\text{tot}}} \times 100 \quad (2.27)$$

Eq. (2.27) represents the percentage ratio between the reactant mass flow rate through the electrode (\dot{m}_{el}) and the total mass flow rate (\dot{m}_{tot}).

This parameter was assumed as indicative of fuel cell performance and for the reference cell we found $\psi = 0.58$.

For each selected flow-field corresponding to the i th active area, the ψ_i value was calculated and plotted versus active area to monitor the selection procedure response varying the constrains range as shown in Fig. 3. Three different runs were performed changing the allowed module repetition number, N , in the following ranges: 7–11, 9–13 and 11–16. The flow-field with a ψ close to that one of the reference cell was considered the best solution. As it can be seen the method, with the imposed constrains, is highly sensitive to parameter N . Increasing the minimum N flow-fields with greater pressure drop are selected and the ψ value increases due to the transition from RS to MS. Then, to have a ψ value near to 0.58 by changing only the N constrains we must select a low N for great area and high N for small area cell.

3. Results and discussion

The method was applied to scale up a serpentine flow-field from 5 cm² (lab reference cell, Fig. 2) to a 125 cm² active area cell using different flow-field type (SS, RS and MS, Fig. 4).

The used MAIN inputs are listed in Table 3, while the channel depth (HCAN) and the rib width (LCOS) were fixed to 1 mm.

For the i th AMEA size the maximum inlet area $A_{\text{in}_{\text{max}}}$, was set according to Eq. (2.5) where k was fixed equal to 1, the $A_{\text{in}_{\text{ref}(i)}}$ value is calculated by MAIN using Eq. (2.2) and sent to the FGS.

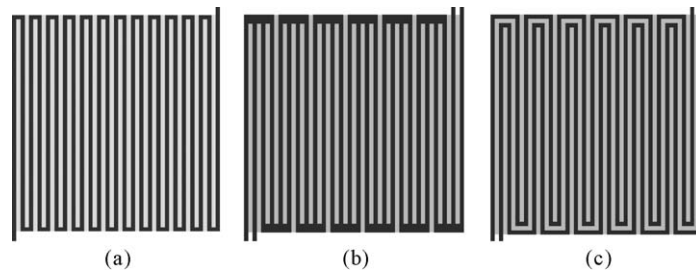


Fig. 4. Sketch of serpentine flow-field types: (a) simple serpentine, (b) n -ribbed-serpentine, (c) n -multiple serpentine. ψ behaviour vs. cell active area for different N range values.

The SGS selection criterion was assigned as follows (see Eqs. (2.11)–(2.17):

$$1.0 \leq \text{LCAN}_i \leq 2.5, \quad 0.50 \leq \chi_i \leq 0.65,$$

$$N = 11, 13, 16, \quad 0.88 \leq \zeta_i \leq 1.19,$$

$$\text{Coll} \leq 3(\text{RS}), \quad \text{Coll} > 3(\text{MS})$$

Fig. 5(a)–(c) shows the obtained α , β , γ scale factor versus active area diagrams, they give an immediate idea about the changing of the FGPs, DCs and FDQ respect to the reference factors value, namely the unit. In fact, fixing the desired scaled-up AMEA size the diagrams furnish all the information needed for flow-field construction and the main fluid-dynamic and active area design characteristics.

Fig. 5(a) shows that simple serpentine has to be taken into consideration for small size active area cells only (up to 15 cm²). In fact, increasing the active area size, the flow rate proportionally raises, but the limitation of maximum channel width should cause a dramatic pressure drop increase. So that, a serpentine channel sub-division is necessary. The possible solutions for higher active area are the RS flow-field from 15 up to 26 cm², and the MS flow-field up to 125 cm². Moreover, Fig. 5(b) and (c) shows the MEA DCs and FDQ behaviour, respectively.

In Table 4, the scale factors for a 100 cm² active area cell, derived from Fig. 5(a)–(c), are reported. Multiplying these scale factors by the correspondent reference parameters (Table 5) the scaled-up cell parameter values (100 cm²) were obtained (Table 6). The residual parameters that are

Table 3
MAIN input parameters

Input parameters	
AMEA _{max} (mm ²)	125
AMEA _{min} (mm ²)	6
ΔAMEA (mm ²)	1
Operative conditions parameters	
J (mA cm ⁻²)	500
T (°C)	80
p (bar)	Room
RH (%)	100
x	1.5/2

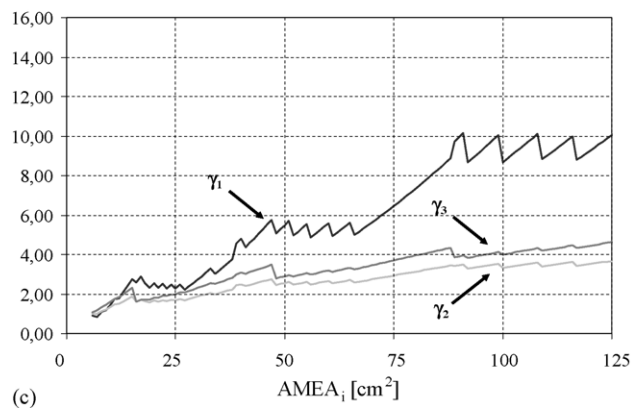
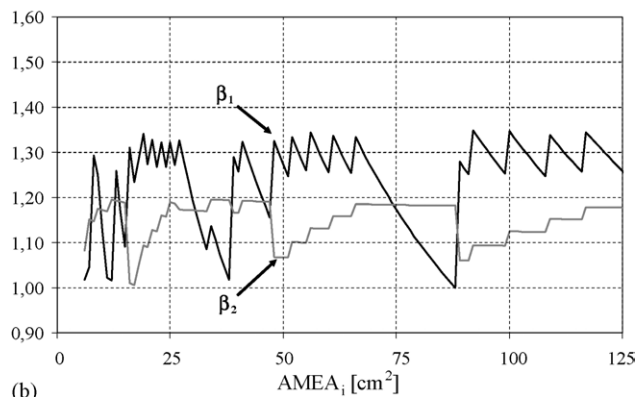
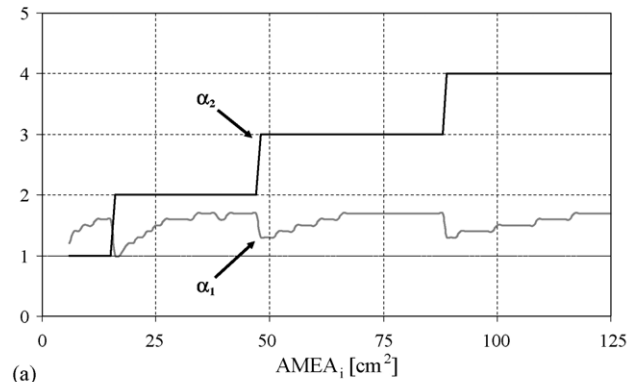


Fig. 5. Scale factor profiles as a function of the active area cell: (a) α_1 , α_2 ; (b) β_1 , β_2 ; (c) γ_1 , γ_2 .

Table 4
100 cm² active area cell scale factors

α	1.50
α_2	4.00
β_1	1.35
β_2	1.125
γ_1	8.677
γ_2	3.333
γ_3	4.000

Table 5
reference 5 cm² parameter values

LCAN (mm)	1
NDIV	1
ζ	0.88
χ	0.54
Δp (mbar)	9.59
v_{med} (m s ⁻¹)	3.32
Re	82.54

Table 6
100 cm² parameter values

LCAN (mm)	1.50
NDIV	4
ζ	1.19
χ	0.61
Δp (mbar)	83.21
v_{med} (m s ⁻¹)	11.06
Re	330.16

not listed in the tables can be easily calculated by equations reported in Appendix A.

4. Conclusions

An automated computer aided method to scale up a fuel cell flow-field was developed. This method utilised an algorithm to generate possible flow-field designs on the basis of the imposed geometrical constraints and to select that one matching the fluid dynamic target. To verify the validity of the method it was applied to a sample case by scaling up a 5 cm² active area lab cell up to 125 cm², and the generated flow-field designs were analysed by computational fluid dynamics. For the selection of a single solution the parameter ψ [2] that accounts for flow distribution was used as a target function, although other selection criteria could be considered. Analysis of obtained results versus constraint variation indicates that the evolved computer aided flow-field design method is a useful tool. Further work is necessary to calibrate the criteria. Work is in progress for experimental validation of the obtained results and for the extension of the method to other flow-field types and geometry.

Appendix A

- Flow-path generation parameters

$$\text{Coll} = \text{NDIV LCAN} + \delta(\text{NDIV} - 1)\text{LCOS},$$

$$\delta = 1 \text{ for MS; } \delta = 0 \text{ for RS}$$

$$\text{Lser} = \text{NDIV LCAN} + (\text{NDIV} - 1)\text{LCOS}$$

$$\text{Lung} = \text{Hmea} - 2\text{Coll}$$

$$N = \text{int} \left(\frac{\text{LMEA} + \text{LCOS}}{\text{Lser} + \text{LCOS}} \right) + \delta$$

$$\text{Lmea} = (N \text{NDIV}) \text{LCAN} + (N \text{NDIV} - 1)\text{LCOS}$$

$$\text{Hmea} = \frac{\text{AMEA}}{\text{Lmea}}$$

- Design coefficients

$$\xi = \frac{A_{lib}}{\text{NDIV LCAN}}$$

$$\zeta = \frac{\text{Lmea}}{\text{Hmea}}$$

$$\chi = \frac{A_{lib}}{\text{AMEA}}$$

$$A_{lib} = A_{cent} + A_{coll} + A_{in,out}$$

$$A_{cent} = N \text{NDIV LCAN Lung}$$

$$A_{in,out} = 2(\text{LCAN NDIV Coll})$$

$$A_{coll} = 2 \left[(\text{NDIV LCAN})^2 + (\text{NDIV} - 1) \text{NDIV} \right. \\ \left. \times (\text{LCAN LCOS}) + \left(\frac{\text{NDIV LCAN LCOS}}{2} \right) \right] \\ \times (N - 1)$$

- Fluid dynamic quantities

$$v_{med} = \frac{\dot{m}}{\rho A_{in}} = \frac{\dot{m}}{\rho(\text{LCAN HCAN NDIV})}$$

$$D_h = \frac{4A_{cross}}{P_{ch}} = 2 \frac{\text{LCAN HCAN}}{\text{LCAN} + \text{HCAN}}$$

$$\text{Re} = \frac{\rho v_{med} D_h}{\mu} = \frac{2\dot{m}}{\mu \text{NDIV}(\text{LCAN} + \text{HCAN})}$$

$$\Delta p_{sc} = \lambda \text{Re}^2 \frac{\mu^2}{2\rho D_h^3} \xi = \lambda \frac{\dot{m}}{4\rho} \frac{\text{LCAN} + \text{HCAN}}{(\text{LCAN HCAN})^3 \text{NDIV}^2} \xi$$

$$\Delta p_{\text{cm}} = \beta \frac{\rho v_{\text{med}}^2}{2}$$

$$\Delta p_{\text{tot}} = \Delta p_{\text{sc}} + \Delta p_{\text{cm}}$$

References

- [1] G. Giacoppo, G. Squadrito, F. Urbani, E. Passalacqua, M. Badami, Proceedings of the HYPOTHESIS V, Porto Conte, Italy, September 7–10, 2003, pp. 707–716.
- [2] H. Dohle, R. Jung, N. Kimiaie, J. Mergel, M. Müller, J. Power Sources 124 (2003) 371–384.
- [3] A. Kazim, H.T. Liu, P. Forges, J. Appl. Electrochem. 29 (1999) 1409–1416.
- [4] O. Barbera, G. Giacoppo, F. Urbani, G. Squadrito and E. Passalacqua, Int. J. Hydrogen Energy, submitted for publication.
- [5] D.P. Wilkinson, O. Vanderleeden, in: W. Vielstich, A. Lamm, H.A. Gastaiger (Eds.), Handbook of Fuel Cells, vol. 3, Wiley, UK, 2003 (Chapter 27).